The yeast S phase checkpoint enables replicating chromosomes to bi-orient and restrain spindle extension during S phase distress

Jeff Bachant, Shannon R. Jessen, Sarah E. Kavanaugh, and Candida S. Fielding

Department of Cell Biology and Neuroscience, University of California, Riverside, Riverside, CA 92521

The budding yeast S phase checkpoint responds to hydroxyurea-induced nucleotide depletion by preventing replication fork collapse and the segregation of unreplicated chromosomes. Although the block to chromosome segregation has been thought to occur by inhibiting anaphase, we show checkpoint-defective *rad53* mutants undergo cycles of spindle extension and collapse after hydroxyurea treatment that are distinct from anaphase cells. Furthermore, chromatid cohesion, whose dissolution triggers anaphase, is dispensable for S phase checkpoint arrest. Kinetochore–spindle attachments are required to prevent spindle extension during replication blocks, and chromosomes with two centromeres or an origin of replication juxtaposed to a centromere rescue the *rad53* checkpoint defect. These observations suggest that checkpoint signaling is required to generate an inward force involved in maintaining preanaphase spindle integrity during DNA replication distress. We propose that by promoting replication fork integrity under these conditions Rad53 ensures centromere duplication. Replicating chromosomes can then bi-orient in a cohesin-independent manner to restrain untimely spindle extension.

Introduction

During mitosis, replicated chromosomes align on a bipolar mitotic spindle and are segregated to daughter cells. In most eukaryotes, chromosome replication and segregation are restricted to separate cell cycle phases by a defined G_2/M transition. However, in budding yeast, DNA replication and spindle assembly are initiated simultaneously. After the G_1/S transition, two kinesin motors, Cin8 and Kip1, have been implicated in forming the preanaphase spindle by pushing apart antiparallel arrays of microtubules (MTs) that inter-digitate between duplicated spindle pole bodies (SPBs). After the spindle poles separate, Cin8 and Kip1 continue to generate an outward force that prevents spindle collapse and drives the dramatic fivefold extension of the spindle that segregates chromosomes during anaphase (Saunders and Hoyt, 1992). Thus, budding yeast face the unusual challenge of preventing inappropriately timed spindle extension while S phase is in progress.

In an unperturbed cell cycle, regulation of preanaphase spindle length is achieved through two processes. First, the outward force of Cin8 and Kip1 is balanced by motors that promote spindle contraction (Saunders et al., 1997). Second, cohesion between replicated chromatids allows the pulling of bi-oriented kinetochores (KTs) toward opposite spindle poles to generate a form of traction that limits spindle extension. Yeast centromeres (*CENs*) replicate early in S phase, and DNA synthesis is completed before SPBs separate (McCarroll and Fangman, 1988). This timing ensures that, similar to the situation in other eukaryotes, chromatid pairs engage the spindle in a bipolar fashion during spindle assembly. Once all chromatids align, an inhibitory signal from the spindle checkpoint that monitors bi-orientation is relieved. The anaphase-promoting complex (APC) then targets Pds1/securin for ubiquitin-mediated degradation (Cohen-Fix et al., 1996). Pds1 proteolysis allows Esp1/separin to cleave the Mcd1/Scc1 cohesin subunit, triggering chromatid disjunction and spindle elongation (Ciosk et al., 1998).

Additional mechanisms are necessary to couple spindle extension to anaphase onset when the relative timing of S phase and spindle assembly is perturbed. After treatment with the ribonucleotide reductase inhibitor hydroxyurea (HU), for example, two protein kinases, Mec1 (homologue of vertebrate ATM/ATR) and Rad53 (homologue of vertebrate Chk2), control S phase checkpoint responses that coordinate chromosome replication and segregation. One facet of the S phase checkpoint promotes DNA synthesis in the face of nucleotide depletion by preventing fork collapse and by delaying the firing of origins

Correspondence to Jeff Bachant: jeffbach@citrus.ucr.edu

Abbreviations used in this paper: APC, anaphase-promoting complex; *CEN*, centromere; HU, hydroxyurea; KT, kinetochore; MT, microtubule; SPB, spindle pole body; WT, wild-type.

The online version of this article includes supplemental material.

The Journal of Cell Biology, Vol. 168, No. 7, March 28, 2005 999–1012
http://www.jcb.org/cgi/doi/10.1083/jcb.200412076

of replication that are activated in mid to late S phase (Santocanale and Diffley, 1998; Lopes et al., 2001). Another facet controls a cell cycle arrest mechanism that prevents spindle extension (Allen et al., 1994; Weinert et al., 1994). Due to the apparent similarity of spindle extension in HU-treated *mec1* and *rad53* mutants to anaphase spindle elongation, it has been thought that the S phase checkpoint prevents spindle extension by preventing anaphase entry. In response to various forms of DNA damage that do not overtly stall DNA replication, Mec1 has in fact been shown to block anaphase through two pathways that make Pds1 resistant to APC proteolysis. One pathway, regulated by Rad53, prevents Pds1 recognition by the APC specificity factor Cdc20 (Agarwal et al., 2003). The other pathway, controlled by the Chk1 kinase, phosphorylates Pds1 to block ubiquitination (Wang et al., 2001). However, cell cycle arrest after HU treatment is independent of Pds1, suggesting an alternative mechanism to Pds1 stabilization restrains spindle extension during early S phase (Yamamoto et al., 1996; Clarke et al., 1999, 2003). The nature of this mechanism remains an unresolved issue in yeast cell cycle control.

Here, we present evidence that the S phase checkpoint controls cell cycle arrest not by inhibiting anaphase but by allowing the bi-orientation of replicating chromosomes to generate an inward force within the spindle that prevents extension during S phase distress. Cell imaging reveals that HU-treated *rad53* mutants undergo cycles of spindle extension and collapse that are dissimilar to anaphase spindle elongation. In addition, S phase checkpoint arrest is independent of cohesin, indicating restraint of spindle extension during S phase is distinct from inhibition of anaphase. Three observations suggest that bipolar chromosome attachments provide a force to prevent defective extension during HU arrest and that Rad53 plays a fundamental role in promoting these connections. First, mutants defective for the KT proteins Ask1, Mif2, Ndc10, and Ndc80 and the KT regulator Ipl1 exhibit spindle extension after HU treatment. Second, a dicentric chromosome rescues spindle extension in HU-treated *rad53* cells. Third, introducing as few as three minichromosomes where an origin of replication is placed in close proximity to a *CEN* is sufficient to block the *rad53* spindle extension phenotype. These findings suggest a model in which the early replication timing of yeast *CENs* is a functionally significant aspect of cell cycle control. According to this view, the conserved role of checkpoint signaling in stabilizing DNA replication complexes ensures *CEN* duplication during S phase distress. Replicating chromosomes can then biorient and generate the traction necessary to restrain untimely spindle extension.

Results

Spindle extension in *rad53* mutants treated with HU

We consistently noticed differences between spindle extension in *mec1* and *rad53* mutants treated with HU and anaphase spindle elongation, prompting a detailed examination of the S phase checkpoint cell cycle arrest defect. The *rad53-21* allele was chosen for this analysis because *rad53-21* is proficient for the essential function of *RAD53* but exhibits an S phase checkpoint defect equivalent to a *rad53* deletion (Desany et al., 1998). Wild-type (WT) and *rad53-21* cells were synchronized in G_1 and released in the presence or absence of 200 mM HU. Spindle morphology was examined using tubulin-GFP and a *CEN*-proximal GFP chromosome tag (*TRP1-GFP*; Straight et al., 1997). WT cells arrested with a 1–2-μm spindle and a single *TRP1-GFP* dot adjacent to one SPB (Fig. 1 A). In contrast, many *rad53-21* cells displayed spindle extension, frequently characterized by reduced tubulin intensity in the central spindle, suggesting collapse, breakage, or disassembly. These aberrant spindles were only observed after HU treatment; spindle elongation in *rad53-21* cells in the absence of HU was indistinguishable from WT controls (Fig. 1 D and not depicted). During *rad53-21* spindle extension, *TRP1-GFP* was visualized as a single dot closely associated with either SPB (Fig. 1 A); DAPI staining confirmed the majority of DNA was segregated on the spindle (Fig. 1 B). To provide a more quantitative assessment of spindle extension, a GFP-tagged SPB protein was used to measure pole separation in HU-treated *rad53-21* mutants. Using 3 μm as a minimum length for an extended spindle, ∼40–50% of *rad53-21* cells exhibited spindle extension with similar kinetics to anaphase spindle elongation in an unperturbed cell cycle (Fig. 1, C and D). Most spindles did not extend beyond 5 μm, far shorter than the ∼10-μm spindles characteristic of complete anaphase extension (Fig. 1 C). Thus, spindle extension in HU-treated *rad53* mutants is variable, incomplete, and accompanied by perturbations to spindle morphology.

Rad53 is required to maintain mitotic Cdk1 activity after DNA damage checkpoint activation (Sanchez et al., 1999). To determine if Rad53 functioned similarly in S phase, WT and *rad53-21* Clb2-HA strains were released from G_1 in the presence or absence of HU. Clb2-Cdk1 was recovered by immunoprecipitation. Both WT and *rad53* cells accumulated Clb2-Cdk1 activity during the replication block, although at reduced rates compared with untreated controls (Fig. 1 E). Thus, Rad53 is not required to maintain Clb2-Cdk1 activity during HU arrest.

rad53 mutants treated with HU undergo dynamic alterations in spindle length

We continued our analysis of the *rad53* S phase checkpoint defect by visualizing spindle extension using live cell imaging (Videos 1–5, available at http://www.jcb.org/cgi/content/full/jcb.200412076/DC1). WT and *rad53-21 SPC42-GFP* strains were released from G_1 arrest into 200 mM HU media. Filming was initiated once spindle extension was occurring in ∼25% of the population, allowing visualization of the initial extension of the spindle in some cells and subsequent changes once spindle extension had occurred in others. In HU-arrested WT cells, spindle length remained relatively constant at ∼2 μm, although translocations of the spindle within the cell were observed (Fig. 2 A). Spindle translocations were also observed in *rad53* mutants, but were accompanied by SPB separation at rates comparable to the 0.5 μm/min observed during the rapid phase of anaphase B (Straight et al., 1997; Fig. 2, B–D). Unexpectedly, spindle extension was in fact reversible, with SPBs contracting at rates similar to the rate of extension. This cycle was variable,

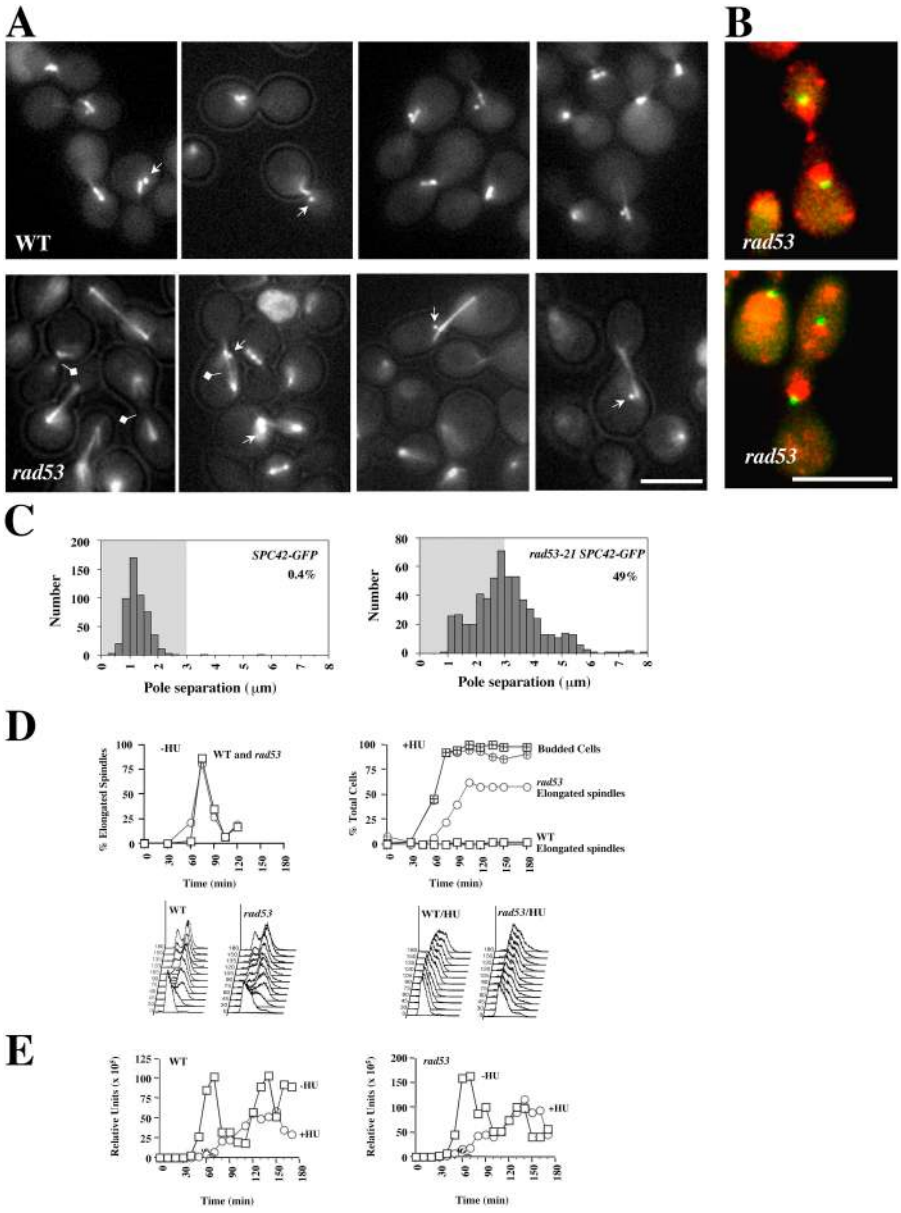

Figure 1. **Spindle extension in HU-treated *rad53-21* mutants.** (A) WT (JBY430) and *rad53-21* (JBY1201) *GFP-TUB1 TRP1-GFP* cells were released from G_1 into 200 mM HU and visualized by GFP fluorescence and low intensity bright-field illumination after 90 min. Arrows, *TRP1-GFP* foci; pointers, reduced tubulin-GFP in *rad53* spindles. Bar, 5 μm. (B) Pseudo-colored images of chromatin (DAPI; red) and spindle poles (*SPC42-GFP*; green) in HU-treated *rad53-21* mutants (JBY1274) 2 h after release from G_1 into 200 mM HU. Bar, 5 μm. (C) Spindle length in HU-arrested WT (JBY1129) and *rad53-21* (JBY1274) *SPC42-GFP* cells. The distance between Spc42-GFP foci was measured in 500 cells 2 h after release from G_1 into 200 mM HU. The percentage of spindles ≥3 μm is indicated. (D) Spindle extension kinetics in WT (Y300) and *rad53-21* (Y301) strains. Time points from cultures released from G_1 with (right) or without (left) 200 mM HU were processed for FACS and α-tubulin immunofluorescence. The percentage of spindles ≥3 μm (open squares, WT; open circles, *rad53-21*) and budded cells (hatched square, WT; hatched circle, *rad53-21*) was determined. (E) Clb2-Cdk1 activity in WT (JBY012; left) and *rad53-21* (JBY013; right) cells. Cells harboring Clb2-$HA_{3\times}$ were released from G_1 in the presence (circles) or absence (squares) of 200 mM HU, and histone H1 kinase activity in α-HA immunoprecipitates was quantified.

with seemingly stochastic conversions between extension and collapse. These dynamics account for the continuum of spindle lengths in HU-treated *rad53* cells and are distinct from unidirectional spindle elongation during anaphase.

Cohesin is not required to prevent spindle extension during S phase arrest

Yeast mutants defective for APC-mediated Pds1 degradation cannot disjoin chromatids and arrest with an ~2–3-μm metaphase spindle. The importance of cohesion in preventing spindle extension can be observed using APC mutants that are also defective for cohesion, as these cells undergo spindle extension even though Pds1 is stabilized (Michaelis et al., 1997). Although Pds1 is not required to prevent spindle extension during S phase checkpoint arrest, cohesin is deposited on chromosomes at an HU replication block (Blat and Kleckner, 1999). Thus, cohesion at early replicating *CEN* regions could prevent spindle extension at a point when Mcd1/Scc1 was not yet susceptible to cleavage. Alternatively, S phase checkpoint arrest could occur through a cohesin-independent mechanism. To distinguish between these scenarios, we compared the ability of cohesion-defective *scc1-73* mutants to restrain spindle extension during either S phase checkpoint arrest induced by HU or during metaphase arrest induced by inactivation of the APC component Cdc23. WT, *rad53-21*, and *scc1-73* mutants were released from a G_1 block into 200 mM HU media at a *scc1-73* nonpermissive temperature. Whereas *rad53-21* initiated spindle extension between 60–90 min, *scc1-73* mutants arrested with normal preanaphase spindles (Fig. 3; Guacci et al., 1997). However, when *cdc23-1*, *cdc23-1rad53-21*, and *cdc23-1scc1-73* cells were released in the absence of HU, we observed a reciprocal pattern where *cdc23rad53-21* mutants arrested normally but *cdc23-1scc1-73* exhibited spindle extension. Thus, Mcd1/Scc1 does not couple spindle extension to anaphase onset during S phase checkpoint arrest.

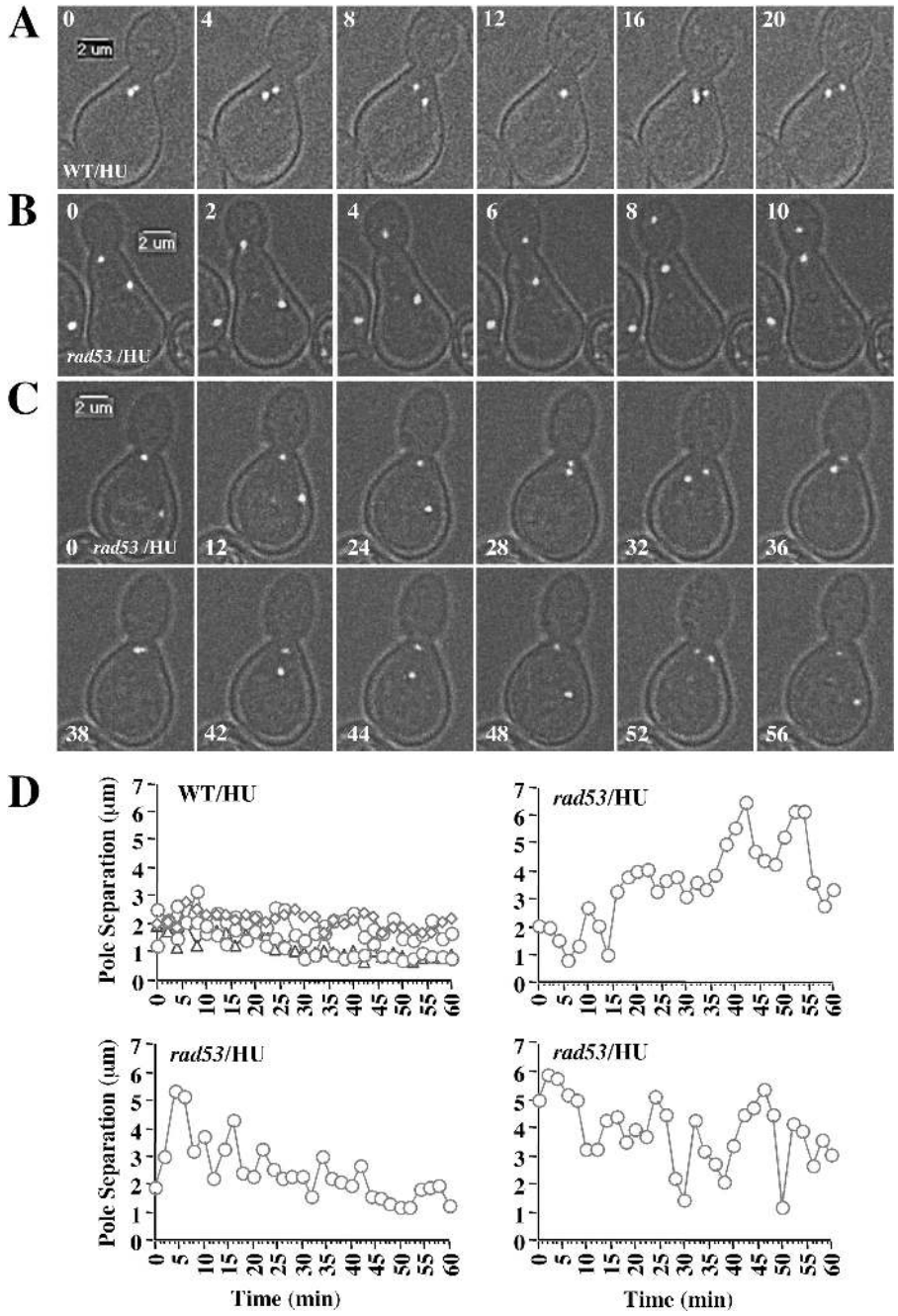

Figure 2. **Spindle dynamics in *rad53-21* mutants.** WT (JBY1129) and *rad53-21* (JBY1274) *SPC42-GFP* strains were released from G_1 into 200 mM HU. Cells were prepared for imaging 75–90 min after release. Stacks of Spc42-GFP images were acquired every 2 min. Numbers indicate lapsed time. (A) 20-min time-lapse sequence for a WT cell. (B and C) SPB extension and collapse in two HU-treated *rad53-21* cells. (D) Graphs depicting changes in spindle length over time for four WT and three *rad53-21* cells.

Chromosome attachment to the spindle is required to restrain S phase spindle extension

To define the cohesin-independent forces restraining spindle extension during S phase, we conducted a genetic screen for mutants exhibiting HU sensitivity and extended spindles after HU treatment (Esh$^-$ phenotype; Alcasabas et al., 2001). Interestingly, mutant alleles of two genes implicated in KT function (*ASK1* and *SMT4/ULP2*) were identified. *ASK1* encodes a component of the *CEN*-binding Dam1/DDD/DASH complex (Li et al., 2002), whereas *SMT4* encodes an isopeptidase that deconjugates the ubiquitin-like SUMO protein (Li and Hochstrasser, 2000). *SMT4* was isolated as a suppressor of a mutation in the KT protein Mif2, suggesting *SMT4* might function in a pathway regulating Mif2 function (Meluh and Koshland, 1995). Indeed, we identified Mif2 as a Smt4 binding partner in a two-hybrid screen, providing another connection between these proteins (Fig. 4 C). *smt4-3* and *ask1-1* mutants isolated in the Esh$^-$ screen failed to recover from HU treatment, although the severity of this defect was less than that of *rad53-21* (Fig. 4 A). Using the criteria established for *rad53*, ~25% of *smt4-3 SPC42-GFP* cells and ~10% of *ask1-1 SPC42-GFP* cells released from G_1 into 200 mM HU media showed an extended spindle phenotype (Fig. 4 B).

The results from the Esh$^-$ screen are consistent with a role for the KT in preventing spindle extension during HU ar-

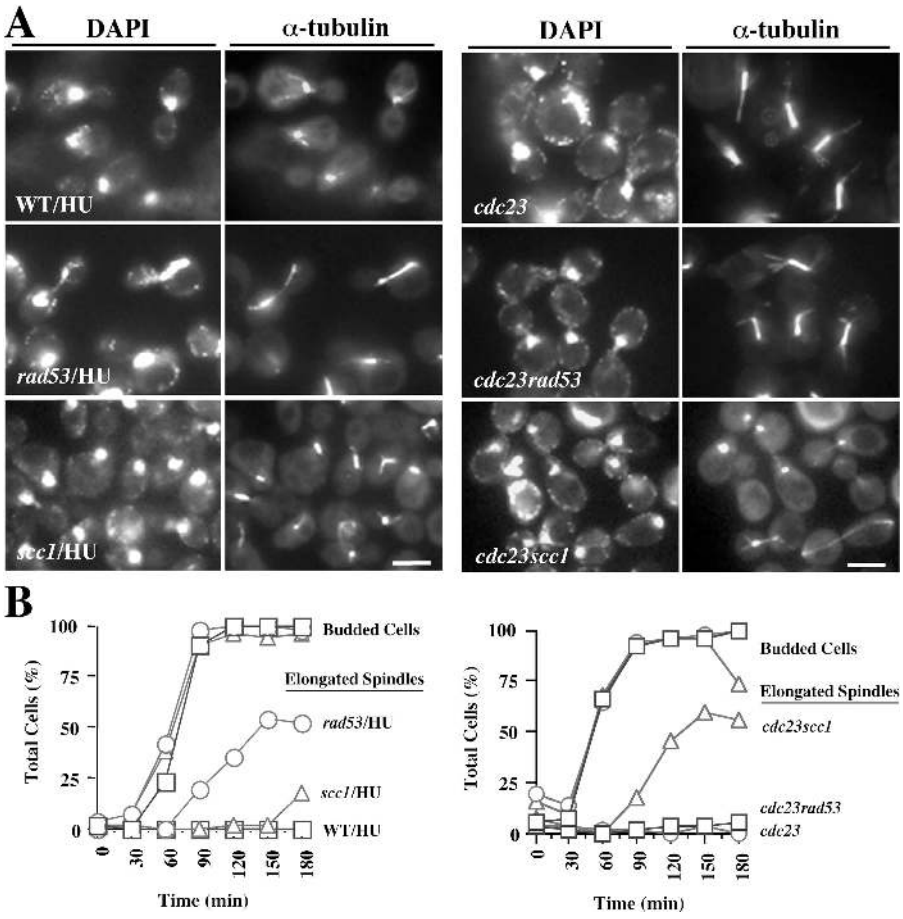

Figure 3. ***SCC1* is not required to prevent spindle extension during HU arrest.** WT (Y300), *rad53-21* (Y301), and *scc1-73* (JBY585) strains were released from G_1 into 200 mM HU at 35°C. *cdc23-1* (JBY622), *cdc23-1rad53-21* (JBY623), and *cdc23-1scc1-73* (JBY1305) strains were released at 35°C in the absence of HU. (A) Spindle (α-tubulin) and chromosome (DAPI) morphology in HU- or *cdc23*-arrested strains 2.5 h after G_1 release. Bars, 5 μm. (B) Kinetics of spindle extension and budding. (left) HU-arrested strains (squares, WT; circles, *rad53-21*; triangles, *scc1-73*). (right) *cdc23-1*–arrested strains (squares, *cdc23-1*; circles, *cdc23-1rad53-21*; triangles, *cdc23-1scc1-73*).

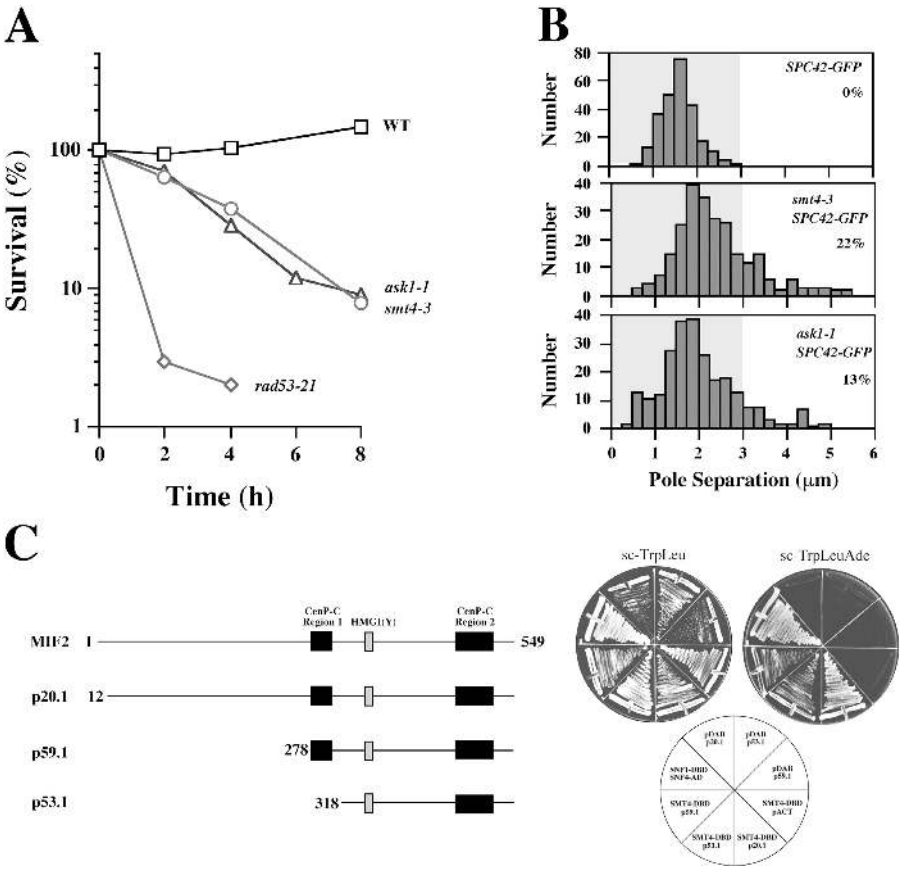

Figure 4. **Analysis of Esh⁻ mutants.** (A) Cell survival after HU treatment. Cultures of WT (Y300; squares), *smt4-3* (JBY047; triangles), *ask1-1* (JBY368; circles), and *rad53-21* (Y301; diamonds) cells were exposed to 200 mM HU. At the indicated times, aliquots were plated for cell viability. (B) Spindle length during HU arrest. The distance between Spc42-GFP foci was measured for 250 WT (JBY1129), *smt4-3* (JBY1312), and *ask1-1* (JBY1196) *SPC42-GFP* cells 2.5 h after release from G_1 into 200 mM HU. The percentage of spindles ≥3 μm is indicated. (C) *MIF2* clones isolated as Smt4 two-hybrid interactors. Regions of similarity to CENP-C (black boxes) and the HMGI (Y) domain (gray box) are indicated. pDAB (*GAL4* DNA binding domain [DBD] vector), pACT (*GAL4* activation domain [AD] vector), pSE1111 (*SNF4*-DBD), pJBN84 (*SMT4*-DBD), and *MIF2*-AD clones p20.1, p53.1, and p59.1 were analyzed in the indicated combinations. Growth on Trp⁻Leu⁻Ade⁻ media indicates a two-hybrid interaction.

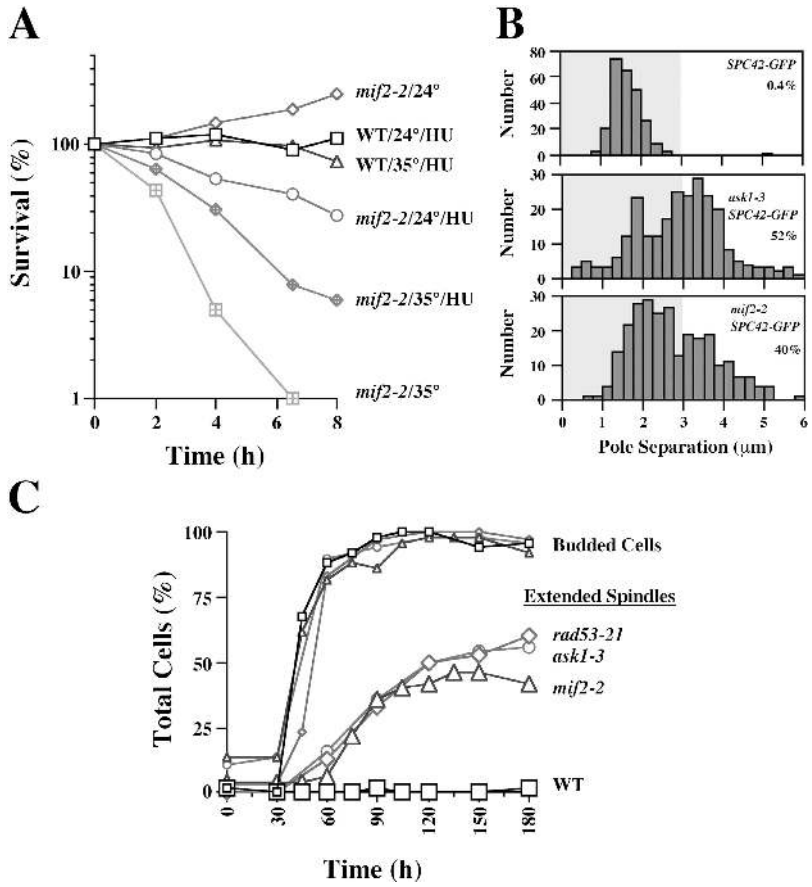

Figure 5. ***MIF2* and *ASK1* restrain spindle extension during HU arrest.** (A) Cell survival in HU-treated *mif2-2* mutants. Cultures of WT (Y300) and *mif2-2* (JBY358) strains were treated ± 200 mM HU at 24 or 35°C. Aliquots were plated to monitor cell viability. Squares, WT/24°C/HU; triangles, WT/35°C/HU; diamonds, *mif2-2*/24°C; circles, *mif2-2*/24°C/HU; hatched diamonds, *mif2-2*/35°C/HU; hatched squares, *mif2-2*/35°C. (B) Spindle length was measured for 250 WT *SPC42-GFP* (JBY1129), *ask1-3 SPC42-GFP* (JBY1325), and *mif2-2* (JBY358) cells 2.5 h after G_1 release into 200 mM HU. The percentage of spindles ≥3 μm is indicated. (C) Kinetics of spindle extension during HU arrest. WT (Y300, squares), *rad53-21* (Y301; diamonds), *mif2-2* (JBY358; triangles), and *ask1-3* (JBY1325; circles) were released from G_1 into 200 mM HU at 35°C. Time points were processed for DAPI and α-tubulin staining.

rest. However, spindle extension in HU-treated *smt4-3* mutants could reflect SUMO regulation of processes unrelated to KT function. Also, the spindle extension phenotype of *ask1-1* is less severe than *rad53-21*. Therefore, we began a more comprehensive analysis of KT-defective strains, beginning with *mif2-2* and *ask1-3* mutants. At a nonpermissive temperature, *ask1-3* cells undergo an aberrant mitosis in which spindles extend in the absence of chromatid disjunction (Li et al., 2002). The failure of chromatids to separate reflects activation of the spindle checkpoint because the delay in sister separation is eliminated in checkpoint-defective *ask1-3mad2*-Δ mutants. Similarly, when *mif2-2 TRP1-GFP* cells were released from G_1 at a nonpermissive temperature, spindle extension was initiated well in advance of *TRP1-GFP* disjunction, and the relative timing of chromatid separation and spindle extension was restored in a *mif2-2mad2*-Δ strain (Fig. S1, available at http://www.jcb.org/cgi/content/full/jcb.200412076/DC1). *mif2-2* mutants showed reduced viability when exposed to HU (Fig. 5 A), and, after release from G_1 into 200 mM HU media at a nonpermissive temperature, ∼40–50% of *mif2-2* and *ask1-3* cells displayed a robust Esh^- phenotype (Fig. 5 B). Spindle extension was initiated with similar timing to *rad53* controls (Fig. 5 C), and, as observed in *rad53* mutants, elongated spindles exhibited diminished tubulin staining in interpolar regions (Fig. 6 A). Thus, Ask1 and Mif2 are required to couple spindle extension to anaphase onset not only during a metaphase block induced by the spindle checkpoint but also during an S phase block induced by HU. This finding is in contrast to the requirements for Mcd1/Scc1, which is only manifested once the bulk of S phase is complete, and for Rad53, which is only observed during S phase arrest (Fig. 3).

Although HU-treated *rad53*, *ask1*, and *mif2* mutants all exhibit untimely spindle extension during S phase, there was an apparent difference between these strains in the association of replicating chromosomes with the spindle. During spindle extension in *rad53-21* cells, chromosomes partitioned equivalently between SPBs (Fig. 1 B). In contrast, chromosomes often associated with a single SPB or were distributed unequally along the spindle axis in HU-treated *ask1-3* and *mif2-2* strains (Fig. 6 A). Therefore, we used a *GAL-CEN* transcription readthrough assay as a different assessment of *CEN*–KT complex function in *rad53-21* mutants. In this assay, a *CEN* is placed between a promoter and a reporter gene, creating a barrier to transcription after KT assembly. Mutations that disrupt *CEN* chromatin structure relax this interference, allowing increased reporter gene expression (Doheny et al., 1993). WT and *rad53-21* cells transformed with a minichromosome in which *CEN6* was positioned between the *GAL1/10* promoter and the *URA3* gene (p*GAL-CEN6-URA3*) exhibited a 10–100-fold reduction of growth on galactose media lacking uracil compared with p*GAL-URA3*controls lacking the *CEN6* insert (Fig. 6 B). In contrast, *mif2-2*/p*GAL-CEN6-URA3* and *mif2-2*/p*GAL-URA3* cells showed equivalent growth with or without *URA3* selection, indicating a relief of *CEN* interference. Thus, an

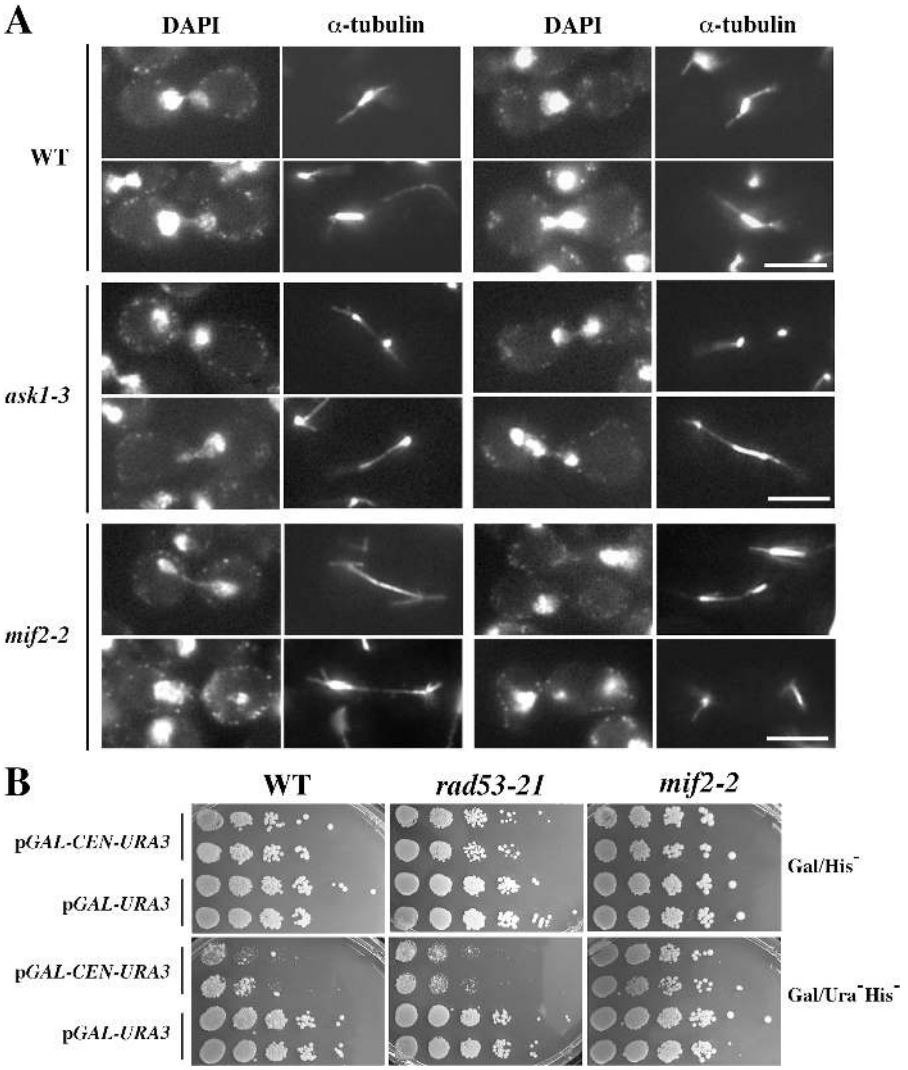

Figure 6. **Analysis of spindle morphology in HU-treated *ask1* and *mif2* mutants and *CEN* function in *rad53* mutants.** (A) Spindle extension after activation of the S phase checkpoint. 2.5 h after release from G_1 to 200 mM HU at 35°C, DAPI and α-tubulin images were obtained for WT, *ask1-3*, and *mif2-2* strains. Bars, 5 μm. (B) *CEN* transcription assay. 10-fold serial dilutions of WT (Y300), *rad53-21* (Y301), and *mif2-2* (JBY358) strains transformed with p*GAL-CEN6-URA3* or p*GAL-URA3* were spotted onto Gal/His⁻ and Gal/His⁻Ura⁻ galactose media. Growth was assayed after 4 d at 28°C. Growth on His⁻ media selects for the plasmid; His⁻Ura⁻ plates reveal the extent of *CEN* interference with *URA3* expression.

important distinction between *mif2* and *rad53* mutants is that spindle extension in HU-treated *rad53* cells is not accompanied by a detectable defect in *CEN*–KT complex structure or function.

Many KT-defective mutants exhibit perturbations to preanaphase spindle integrity characterized by defective extension (Jones et al., 1999; Goshima and Yanagida, 2000; Enquist-Newman et al., 2001; Janke et al., 2002; Nekrasov et al., 2003). However, there is considerable variability in this phenotype. For example, a recent paper examined a collection of *dam1* mutants and found that different alleles exhibited phenotypes ranging from cell cycle arrest with typical preanaphase spindle morphology to an aberrant arrest accompanied by spindle extension (Cheeseman et al., 2001). This same paper found that *dam1* mutants do not exhibit a loss of spindle integrity during HU arrest. However, based on our results with *ask1-3* and *mif2-2*, we hypothesized that KT mutants exhibiting spindle extension when cell cycle progression was delayed in metaphase might also display extension during HU arrest. To test this hypothesis, we constructed a panel of *cdc23-1* KT-defective double mutants. After release from G_1 at a *cdc23* nonpermissive temperature, we could then compare the effect of a KT-defective mutation on spindle length during either S phase arrest (by adding HU) or metaphase arrest (by withholding HU). It has been proposed that the KT assembles from protein complexes defining inner, medial, and outer KT regions (Cheeseman et al., 2002). Therefore, we examined mutations affecting the inner CBF3 complex (*ndc10-1*, *ndc10-2*, and *ctf13-30*), the medial Ndc80 complex (*ndc80-1*), and the outer Dam1/DDD/DASH complex (*dam1-1* and *duo1-2*).

In the absence of HU, *cdc23-1* mutants arrested with 2–4-μm metaphase spindles (average 2.9 ± 0.6 μm), whereas *cdc23-1* strains released in the presence of HU displayed the shorter spindles typical of S phase checkpoint arrest (average 2.0 ± 0.5 μm; Fig. 7). Both with and without HU treatment, *cdc23-1duo1-2*, *cdc23-1ctf13-30*, and *cdc23-1ndc10-2* strains arrested similarly to *cdc23-1* controls (unpublished data). Thus, these mutants fall in the anticipated class that do not perturb preanaphase spindle integrity. In contrast, *cdc23-1ndc10-1*, *cdc23-1ndc80-1*, and *cdc23-1dam1-1* mutants all displayed spindle extension at the *cdc23* block. Of these, *cdc23-1ndc10-1* and *cdc23-1ndc80-1* mutants also displayed untimely extension after HU treatment. A relatively small population (12%) of *cdc23-1dam1-1* cells treated with HU did in fact exhibit ≥3-μm spindles. However, there was

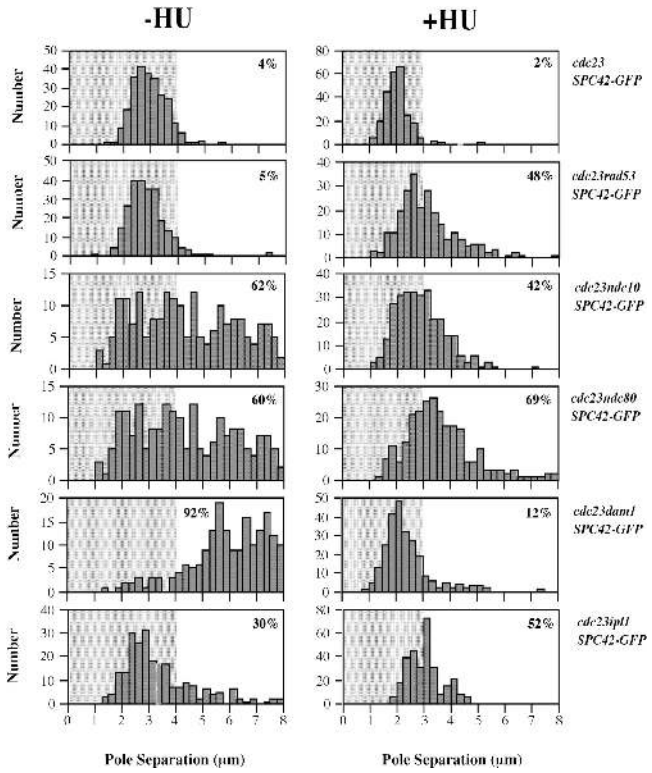

Figure 7. **Spindle extension in KT mutants during HU or metaphase arrest.** *cdc23-1* (JBY1289), *cdc23-1rad53-21* (JBY1293), *cdc23-1ndc10-1* (JBY1367), *cdc23-1ndc80-1* (JBY1363), *cdc23-1dam1-1* (JBY1333), and *cdc23-1ipl1-321* (JBY1357) *SPC42-GFP* strains were released from G_1 ± 200 mM HU at 35°C. After 2.5 h, the distance between Spc42-GFP foci was measured for 250 cells. The percentage of spindles ≥4 μm (−HU) or ≥3 μm (+HU) is depicted.

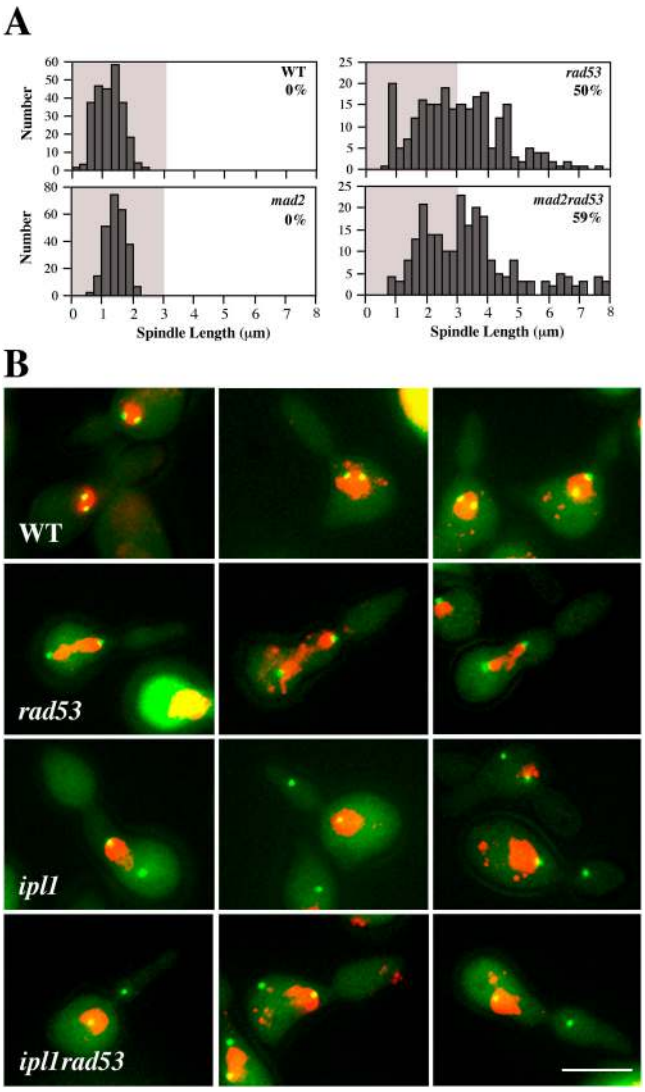

Figure 8. **HU-treated *mad2* and *ipl1* mutants.** (A) Spindle length was measured in 250 WT (Y300), *rad53-21* (Y301), *mad2*-Δ (JBY1393), and *rad53-21mad2*-Δ (JBY1395) cells 2.5 h after release from G_1 into 200 mM HU. The percentage of spindles ≥3 μm is indicated. (B) Pseudocolored images of chromatin (DAPI; red) and spindle poles (Spc42-GFP; green) in HU-treated WT (JBY1129), *rad53-21* (JBY1274), *ipl1-321* (JBY1353), and *ipl1-321rad53-21* (JBY1389) *SPC42-GFP* strains 2.5 h after G_1 release into 200 mM HU. Bar, 5 μm.

much greater requirement for Dam1 after completion of S phase, with 92% of *cdc23dam1-1* cells exhibiting spindle extension.

The aforementioned approach was extended to include mutants defective for the Aurora B homologue Ipl1. Because *rad53* mutants did not appear defective for KT–spindle attachment, the role of Ipl1 was of particular interest because Ipl1 mediates two functions that, although not directly required for chromosomes to connect to the spindle, play important roles in facilitating KT bi-orientation. First, Ipl1 controls a spindle checkpoint response that delays Pds1 proteolysis when KTs are not tensed during spindle attachment (Biggins and Murray, 2001). It is unlikely that this aspect of Ipl1 function prevents spindle extension during HU arrest because checkpoint-defective *mad2*-Δ mutants arrested with normal preanaphase spindles after HU treatment (Fig. 8 A). Ipl1 also promotes bi-orientation by destabilizing monopolar chromatid connections. This function has been illustrated in *cdc6* mutants, which fail to initiate DNA replication and undergo a "reductional" anaphase where unreplicated chromosomes segregate with both poles during spindle extension (Piatti et al., 1995). Chromosomes only associate with a single pole in *cdc6ipl1* double mutants, revealing Ipl1 releases KTs from their initial SPB attachment and redistributes them to both poles during spindle assembly (Tanaka et al., 2002). Consistent with a role for bi-orientation in generating the traction required to restrain spindle extension, *cdc23ip1-321* mutants displayed extended spindles both during metaphase arrest and after HU treatment (Fig. 7). Furthermore, chromatin remained predominately associated with a single pole during spindle extension in HU-treated *ipl1-321* and *rad53ipl1-321 SPC42-GFP* cells (Fig. 8 B). (To observe extension in *ipl1-321* strains it was necessary to preshift the cells to 35°C for 1 h before G_1 release.) First, we conclude that Ipl1 is required for chromosome segregation in HU-treated *rad53* cells; and, second, that a distribution of KT–MT attachments to both spindle poles is necessary to prevent spindle extension during S phase checkpoint arrest.

Juxtaposition of *CEN* and *ARS* sequences rescue spindle extension in *rad53* mutants

One hypothesis to accommodate our observations is that Rad53 promotes a cohesin-independent form of chromosome bi-orien-

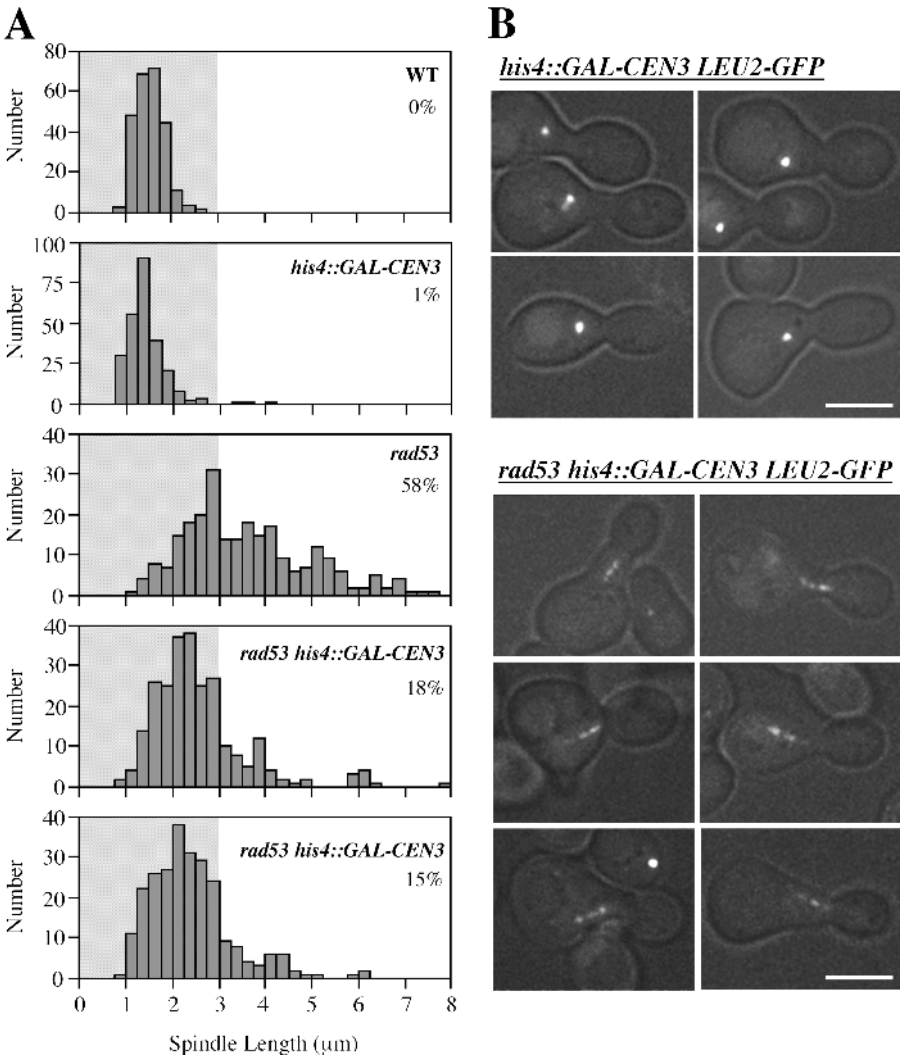

Figure 9. **Dicentric bridging restricts spindle extension in HU-treated *rad53* mutants.** *LEU2-GFP* (JBY541), *his4::GAL-CEN3 LEU2-GFP* (JBY1208), *rad53-21 LEU2-GFP* (JBY1201), and two *rad53-21 his4::GAL-CEN3 LEU2-GFP* segregants (JBY1203 and JBY1206) were propagated in galactose media, placed at G_1 arrest, and released into 200 mM HU glucose media to activate the dicentric. (A) After 2 h, cells were processed for α-tubulin immunofluorescence and spindle length was measured for 250 cells. The percentage of spindles ≥3 μm is indicated. (B) Starting at 90 min after release, GFP-tagged chromatin between the dicentric *CEN*s was visualized by fluorescence. Bars, 5 μm.

tation by ensuring that *CEN*s replicate during HU challenge. If this hypothesis is correct, bridging a dicentric chromosome toward opposite spindle poles might partially substitute for Rad53 in restraining spindle extension. Conditional dicentrics have been constructed in which KT assembly at an exogenous *CEN* can be activated by transferring cells from galactose to glucose media (Thrower and Bloom, 2001). By integrating a GFP chromosome tag between the two *CEN*s (*LEU2-GFP*) on the dicentric it is possible to visualize the bridged chromatin region. We observed that dicentric activation in HU-treated *rad53-21* strains did in fact decrease spindle extension beyond 3 μm (Fig. 9 A). This restriction was accompanied by *LEU2-GFP* becoming extended into a series of punctate foci, suggesting the two KTs were oriented toward opposite poles and placed under tension (Fig. 9 B).

Although budding yeast *CEN*s replicate early in S phase, the origins from which these forks originate are typically located several kilobases away from the *CEN* (Yabuki et al., 2002). If Rad53 promotes *CEN* replication during HU treatment by allowing forks to traverse the distance to the *CEN* without collapsing, we reasoned that reducing this distance might compensate for loss of Rad53 function. Fortuitously, such a juxtaposition of *CEN* and origin sequences is found on circular minichromosome plasmids engineered for transfer of DNA sequences in yeast (Sikorski and Hieter, 1989). The origin sequence (*ARS*) on these minichromosomes is only ∼300 bp distant from the *CEN*. Therefore, we examined the consequences of introducing one, two, three, and four *CENARS* minichromosomes into HU-treated *rad53-21* cells. Remarkably, as few as two *CENARS* minichromosomes reduced spindle extension in HU-treated *rad53-21* mutants by ∼50%, and a further decrease was seen in cells harboring three or four minichromosomes (Fig. 10, A and B). If these minichromosomes suppress *rad53* spindle extension by allowing *CEN* replication, the suppression should require DNA replication and KT assembly. Indeed, the suppression afforded by three *CENARS* minichromosomes after HU treatment was not observed in *dbf4-1* and *dbf4-1rad53-21* cells defective for initiation of DNA replication or in *ndc80-1* and *ndc80-1rad53-21* cells (Fig. 10 C). In contrast, *CENARS* minichromosomes were still able to suppress spindle extension in HU-treated *scc1-73rad53-21* and *mad2-Δrad53-21* strains, indicating this effect did not require cohesion or spindle checkpoint activation. Therefore, reducing the distance between origins of replication and a critical number of *CEN*s is

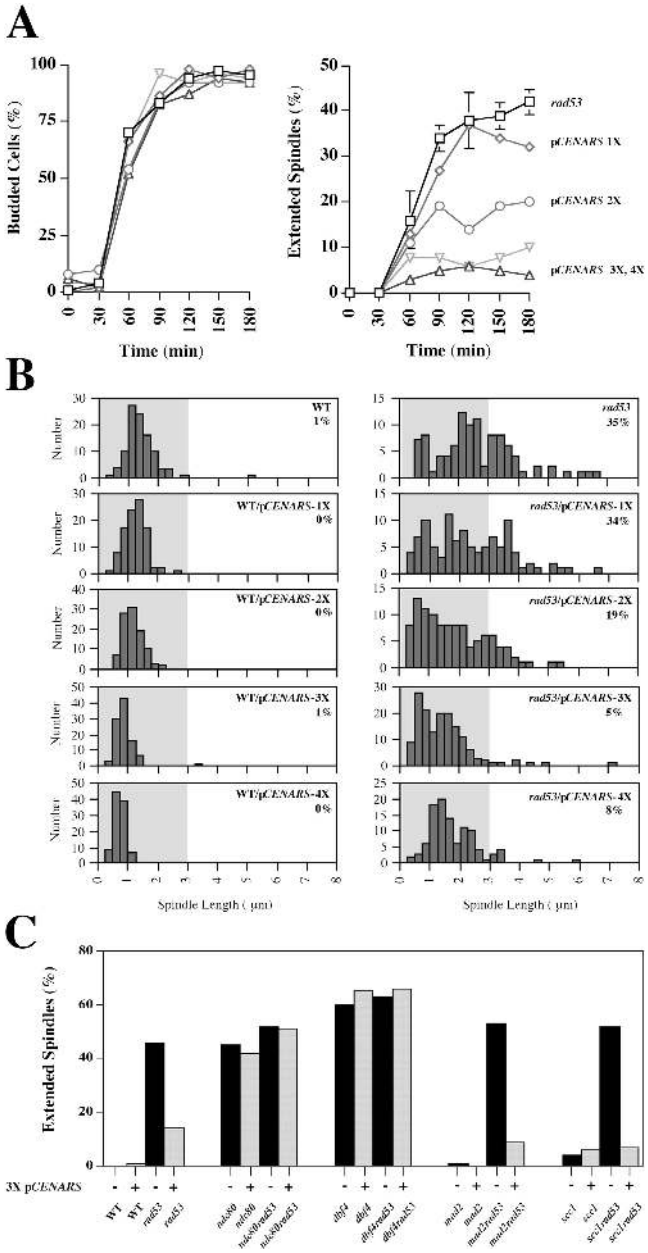

Figure 10. **p*CENARS* minichromosomes suppress spindle extension in HU-treated *rad53* mutants.** WT (JBY1129) and *rad53-21* (JBY1274) *SPC42-GFP-TRP1* strains were transformed with one (pRS413), two (pRS413 and pRS415), or three (pRS413, pRS415, and pRS416) p*CENARS* plasmids (Sikorski and Hieter, 1989). WT (Y300) and *rad53-21* (Y301) were transformed with four p*CENARS* plasmids (pRS413, pRS414, pRS415, and pRS416). Transformants were cultured to maintain the plasmids, arrested in G_1, and released into yeast extract/peptone/dextrose media containing 200 mM HU. Spindle length was measured in 200 cells at the indicated times using Spc42-GFP foci or α-tubulin immunofluorescence. (A) Effect of p*CENARS* dosage on spindle extension in HU-treated *rad53* mutants (right). (left) Budding kinetics. (B) Spindle length distribution in WT and *rad53* mutants after 2.5 h of HU treatment. The percentage of spindles ≥3 μm is indicated. (C) Requirements for p*CENARS* suppression. WT (JBY1129), *rad53-21* (JBY1274), *ndc80-1* (JBY1359), and *ndc80-1rad53-21* (JBY1400) *SPC42-GFP* strains and *dbf4-1* (JBY997), *dbf4-1rad53-21* (JBY1001), *mad2*-Δ (JBY1393), *mad2-Δrad53-21* (JBY1395), *scc1-73* (JBY585), and *scc1-73rad53-21* (JBY1397) strains ± three p*CENARS* plasmids were released from G_1 into 200 mM HU at 35°C. After 2.5 h, the percentage of spindles ≥3 μm was determined for 200 cells.

sufficient to largely restrain spindle extension in the absence of Rad53 signaling.

Discussion

The S phase checkpoint blocks untimely spindle extension, not anaphase entry

The apparent similarity of spindle extension in HU-treated S phase checkpoint mutants to spindle elongation during anaphase has suggested that checkpoint cell cycle arrest is enforced by forestalling anaphase entry. However, we find that there are in fact significant differences between spindle extension in HU-treated *rad53* mutants and anaphase cells. After HU treatment, *rad53* spindles generally do not undergo the complete elongation characteristic of late anaphase. More dramatically, whereas anaphase spindle extension is unidirectional, spindles in HU-treated *rad53* mutants alternate between extension and contraction in length. These aberrant dynamics constitute the only phenotype suggesting an uncoupling of S phase and mitosis has actually occurred, as *rad53* mutants otherwise remained arrested with Clb2-Cdk1 levels similar to checkpoint-proficient controls. The observation that Mcd1/Scc1 is dispensable for restraining spindle extension during HU arrest further highlights the differences between regulation of anaphase and the S phase checkpoint (Fig. 3; Guacci et al., 1997). This observation does not exclude the possibility that the S phase checkpoint has an important role in promoting cohesion so that cells can control anaphase entry once they overcome the replication block. Rather, the important conclusion is that cohesin-independent and -dependent mechanisms operate sequentially to prevent spindle extension. The S phase checkpoint exploits the cohesin-independent pathway, suggesting spindle extension in HU-treated *rad53* mutants reflects a disruption of the forces controlling spindle length rather than a true anaphase spindle movement.

Chromosome bi-orientation generates S phase spindle traction

Chromatid cohesion is normally an important determinant of spindle length because it allows KT bi-orientation to offset the outward forces driving spindle extension. However, because *CENs* replicate early in S phase in *Saccharomyces cerevisiae* (McCarroll and Fangman, 1988), it is possible that KTs attach to the spindle in a bipolar fashion even before establishing cohesion during DNA replication distress. In this case, properties of a *CEN*-spanning replication bubble (such as intertwining of DNA strands) would presumably substitute for cohesion in tolerating tension on the chromosome fiber. KT bi-orientation normally provides the signal to induce anaphase entry. During early S phase, bi-orientation would not necessarily lead to the same outcome because it is unlikely that all chromosomes would be able to bi-orient (see the following section), and the machinery involved in triggering anaphase does not yet appear to be operational (Yamamoto et al., 1996; Clarke et al., 2003). Starting with our Esh$^-$ screen, we in fact identified mutations affecting four KT proteins, Ask1, Mif2, Ndc10, and Ndc80, that engender spindle extension after HU treatment. These pro-

teins participate in interactions that link *CEN* DNA to spindle MTs (Cheeseman et al., 2002), suggesting a mechanical requirement for KT–spindle attachment during HU arrest. The observation that Ipl1 is also required to prevent S phase spindle extension further suggests KTs must connect to the spindle in a bipolar fashion. Thus, the simplest interpretation is that replicating chromosomes generate bipolar spindle traction in a cohesin-independent fashion, and this force is required to appropriately regulate spindle length in HU-arrested cells.

We note that there is considerable variability in whether or not KT-defective mutants exhibit spindle extension during HU arrest. One explanation for this variability is that increasingly severe alleles compromise KT–MT interactions to a point where insufficient traction is generated to restrain extension. In support of this idea, KT-defective mutants exhibiting spindle extension after HU treatment also tend to exhibit extension when arrested in metaphase. Thus, the KT appears to be fulfilling similar roles in both the cohesin-independent and -dependent pathways restraining spindle extension. One apparent exception to this tendency is Dam1. In agreement with a previous paper, we find that Dam1 plays a more prominent role in restricting spindle extension after completion of DNA replication (Cheeseman et al., 2001), suggesting KT–spindle connections are regulated differently or subjected to different forces once cohesion is established.

Spindle length is controlled not only by KT bi-orientation but also by modulating spindle dynamics. Indeed, while this manuscript was under consideration, an independent paper provided evidence that Cin8 and Stu2, a regulator of MT dynamics that promotes spindle extension, accumulate 2–5-fold in *mec1* mutants after HU treatment (Krishnan et al., 2004). Inactivation of Cin8 and Stu2 reduced *mec1* spindle extension, and overproduction of Cin8 forced spindle extension during HU arrest. Using a GFP tag adjacent to *CEN5*, the separation of *CEN*-proximal regions that accompanies KT bi-orientation during metaphase was not observed during HU arrest, prompting a model in which the S phase checkpoint compensates for an inability to bi-orient replicating chromosomes by down-regulating effectors of spindle extension. In an effort to reconcile these findings with our own conclusions, we note that *CENs* on different chromosomes do not replicate uniformly in HU (Yabuki et al., 2002), and variation in *CEN* bi-orientation between chromosomes might be expected. For example, it has been reported that 29% of *CEN15-GFP* cells exhibit bi-orientation after HU treatment (Goshima and Yanagida, 2000). Furthermore, KT bi-orientation during S phase might be difficult to visualize using GFP chromosome tagging if topological intertwining interfered with *CEN* separation. A second consideration is that inhibiting outward force production within the spindle is limited by the requirement to offset spindle collapse (Saunders and Hoyt, 1992). Therefore, we suggest KT–spindle attachments restrict spindle extension during S phase checkpoint arrest, but the inward force afforded by these connections is likely to be reduced compared with metaphase cells. Therefore, it may be important to simultaneously reduce the force driving spindle extension; such an uncoupling of spindle dynamics and chromosome bi-orientation may underlie the cycles of spindle extension and collapse in HU-treated *rad53* mutants documented in this paper.

CEN replication as an effector of S phase checkpoint arrest

Although our data suggests chromosome attachments to the spindle prevent extension during early S phase, several observations indicate checkpoint signaling is unlikely to play a direct role in KT–spindle connections. In particular, the chromatin stretching that accompanies dicentric activation in HU-treated *rad53* mutants argues that KT–MT attachments form and withstand tension. Dicentric activation actually reduces *rad53* spindle extension, suggesting chromosome bridging can provide a surrogate source of traction that compensates for the *rad53* defect. If this interpretation is correct, it may be surprising that we see a >50% rescue of the *rad53* phenotype. As dicentric KTs presumably connect equally to the same or opposite pole, 50% suppression should be maximal. Because Ipl1 is active in HU-treated *rad53* mutants and spindles cycle between extension and collapse, each cell may experience multiple opportunities to bridge the dicentric.

If Rad53 is not required for KT–spindle attachment, how could the S phase checkpoint be involved in generating spindle traction? Our observations suggest similarities between spindle extension in HU-treated *rad53* mutants and the reductional anaphase of DNA replication mutants (Piatti et al., 1995). A recent paper has shown that the origins closest to all 16 *CEN*s do in fact fire after treatment with 200 mM HU and that most *CEN*s have a variable probability of replicating before fork stalling (Yabuki et al., 2002). Therefore, at the time HU-treated *rad53* mutants initiate spindle extension, S phase checkpoint proficient cells would have replicated some, but not all, *CEN* sequences. Because a critical and conserved aspect of Rad53 function is to prevent convergent replication fork collapse (Lopes et al., 2001), a simple model for S phase checkpoint cell cycle arrest is that Rad53 promotes *CEN* replication while spindle assembly is ongoing. After KT assembly, replicating chromosomes could then bi-orient and restrict extension beyond appropriate preanaphase spindle length. This contingency plan would be supplanted as cells overcame the replication interference, established cohesion, and progressed toward metaphase. Our finding that multiple *CENARS* minichromosomes suppress spindle extension in HU-treated *rad53* mutants, and that this suppression requires both initiation of DNA replication and KT function, provides strong support for a model in which Rad53 promotes cell cycle arrest by controlling *CEN* replication. If this model is correct, a key prediction is that the Rad53 substrates involved in preventing spindle extension will prove to be identical to the substrates controlling replication fork stabilization during HU treatment.

It has been known for some time that mammalian cells induced to enter mitosis without completing S phase generate KT fragments that align and segregate on the spindle (Brinkley et al., 1988). Similarly, recent evidence from yeast suggests that the primary role of cohesin in facilitating KT bi-orientation is to allow proper chromosome tensioning; in experimental situations, this function can be supplied by

Table I. **Yeast strains used in this study**

Strain	Genotype	Source
PJ69-4a	*MATa trp1-901 leu2-3,112 ura3-52 his3-200 gal4Δ gal80Δ LYS2::GAL1-HIS3 GAL2-ADE2 met2::GAL7-lacZ*	James et al., 1996
Y300	*MATa his3-11,15 leu2-3,112 trp1-1 ura3-1 ade2-1 can1-100*	Allen et al., 1994
Y301	*MATa rad53-21 his3-11,15 leu2-3,112 trp1-1 ura3-1 ade2-1 can1-100*	Allen et al., 1994
Y916	*MATa HIS3 leu2-3,112 trp1-1 ura3-1 ade2-1 can1-100*	This study
Y917	*MATα his3-11,15 LEU2 trp1-1 ura3-1 ade2-1 can1-100*	This study
JBY012	*MATa CLB2-HA$_{3\times}$ his3-11,15 leu2-3,112 trp1-1 ura3-1 ade2-1 can1-100*	This study
JBY013	*MATa rad53-21 CLB2-HA$_{3\times}$ his3-11,15 leu2-3,112 trp1-1 ura3-1 ade2-1 can1-100*	This study
JBY047	*MATa smt4-3 his3-11,15 leu2-3,112 trp1-1 ura3-1 ade2-1 can1-100*	Bachant et al., 2002
JBY331	*MATa smt4-3 his3-11,15 leu2-3,112 trp1-1 ura3-1 ade2-1 can1-100*	Bachant et al., 2002
JBY358	*MATa mif2-2 his3-11,15 leu2-3,112 trp1-1 ura3-1 ade2-1 can1-100*	This study
JBY368	*MATa ask1-1 HIS3 leu2-3,112 trp1-1 ura3-1 ade2-1 can1-100*	This study
JBY428	*MATa his3-11,15-LacI-GFP-HIS3 leu2-3,112 trp1-1-LacO-TRP1-LEU2 ura3-1 ade2-1 can1-100*	Bachant et al., 2002
JBY430	*MATa his3-11,15-LacI-GFP-HIS3 leu2-3,112 trp1-1-LacO-TRP1-LEU2 ura3-1-TUB1-GFP-URA3 ade2-1 can1-100*	This study
JBY450	*MATa mif2-2 his3-11,15-LacI-GFP-HIS3 leu2-3,112 trp1-1-LacO-TRP1-LEU2 ura3-1 ade2-1 can1-100*	This study
JBY541	*MATa his3-11,15-LacI-GFP-HIS3 leu2-3,112-LacO-LEU2 trp1-1 ura3-1 ade2-1 can1-100*	Bachant et al., 2002
JBY548	*MATa mif2-2 Δmad2::URA3 his3-11,15-LacI-GFP-HIS3 leu2-3,112 trp1-1-LacO-TRP1-LEU2 ura3-1 ade2-1 can1-100*	This study
JBY585	*MATa scc1-73 his3-11,15 leu2-3,112 TRP1 ura3-1 ade2-1 can1-100*	This study
JBY622	*MATa cdc23-1 his3-11,15 leu2-3,112 trp1-1 ura3-1 ade2-1 can1-100*	This study
JBY623	*MATa cdc23-1 rad53-21 his3-11,15 leu2-3,112 trp1-1 ura3-1 ade2-1 can1-100*	This study
JBY997	*MATa dbf4-1 his3-11,15 LEU2 trp1-1 ura3-1 ade2-1 can1-100*	This study
JBY1001	*MATa dbf4-1rad53-21 his3-11,15 LEU2 trp1-1 ura3-1 ade2-1 can1-100*	This study
JBY1129	*MATa his3-11,15 leu2-3,112 trp1-1-SPC42-GFP-TRP1 ura3-1 ade2-1 can1-100*	This study
JBY1196	*MATa ask1-1 his3-11,15 leu2-3,112 trp1-1-SPC42-GFP-TRP1 ura3-1 ade2-1 can1-100*	This study
JBY1201	*MATa rad53-21 his3-11,15-LacI-GFP-HIS3 leu2-3,112 trp1-1-LacO-TRP1-LEU2 ura3-1-TUB1-GFP-URA3 ade2-1 can1-100*	This study
JBY1203	*MATa rad53-21 his4-GAL-CEN3-URA3 his3-11,15-LacI-GFP-HIS3 leu2-3,112-LacO-LEU2 trp1-1 ura3-1-TUB1-GFP-URA3 ade2-1 can1-100*	This study
JBY1206	*MATa rad53-21 his4-GAL-CEN3-URA3 his3-11,15-LacI-GFP-HIS3 leu2-3,112-LacO-LEU2 trp1-1 ura3-1 ade2-1 can1-100*	This study
JBY1208	*MATa his4-GAL-CEN3-URA3 his3-11,15-LacI-GFP-HIS3 leu2-3,112-LacO-LEU2 trp1-1 ura3-1-TUB1-GFP-URA3 ade2-1 can1-100*	This study
JBY1274	*MATa rad53-21 his3-11,15 leu2-3,112 trp1-1-SPC42-GFP-TRP1 ura3-1 ade2-1 can1-100*	This study
JBY1289	*MATa cdc23-1 his3-11,15 leu2-3,112 trp1-1-SPC42-GFP-TRP1 ura3-1 ade2-1 can1-100*	This study
JBY1293	*MATa cdc23-1 rad53-21 his3-11,15 leu2-3,112 trp1-1-SPC42-GFP-TRP1 ura3-1 ade2-1 can1-100*	This study
JBY1305	*MATa cdc23-1 scc1-73 his3-11,15 leu2-3,112 TRP1 ura3-1 ade2-1 can1-100*	This study
JBY1312	*MATa smt4-3 his3-11,15 leu2-3,112 trp1-1-SPC42-GFP-TRP1 ura3-1 ade2-1 can1-100*	This study
JBY1325	*MATa ask1-3 his3-11,15 leu2-3,112 trp1-1-SPC42-GFP-TRP1 ura3-1 ade2-1 can1-100*	This study
JBY1333	*MATa cdc23-1 dam1-1 Δask1::LEU2 his3-11,15-ASK1-myc$_{3\times}$-HIS3 leu2-3,112 trp1-1-SPC42-GFP-TRP1 ura3-1 ade2-1 can1-100*	This study
JBY1345	*MATa cdc23-1 duo1-2 his3-11,15 leu2-3,112 trp1-1-SPC42-GFP-TRP1 ura3-1 ade2-1 can1-100*	This study
JBY1351	*MATa cdc23-1 ctf13-30 his3-11,15 leu2-3,112 trp1-1-SPC42-GFP-TRP1 ura3-1 ade2-1 can1-100*	This study
JBY1353	*MATa ipl1-321 his3-11,15 leu2-3,112 trp1-1-SPC42-GFP-TRP1 ura3-1 ade2-1 can1-100*	This study
JBY1357	*MATa cdc23-1 ipl1-321 his3-11,15 leu2-3,112 trp1-1-SPC42-GFP-TRP1 ura3-1 ade2-1 can1-100*	This study
JBY1359	*MATa ndc80-1 his3-11,15 leu2-3,112 trp1-1-SPC42-GFP-TRP1 ura3-1 ade2-1 can1-100*	This study
JBY1363	*MATa cdc23-1 ndc80-1 his3-11,15 leu2-3,112 trp1-1-SPC42-GFP-TRP1 ura3-1 ade2-1 can1-100*	This study
JBY1367	*MATa cdc23-1 ndc10-1 his3-11,15 leu2-3,112 trp1-1-SPC42-GFP-TRP1 ura3-1 ade2-1 can1-100*	This study
JBY1373	*MATa cdc23-1 ndc10-2 his3-11,15 leu2-3,112 trp1-1-SPC42-GFP-TRP1 ura3-1 ade2-1 can1-100*	This study
JBY1389	*MATa ipl1-321 rad53-21 his3-11,15 leu2-3,112 trp1-1-SPC42-GFP-TRP1 ura3-1 ade2-1 can1-100*	This study
JBY1393	*MATa mad2-Δ::URA3 his3-11,15 leu2-3,112 trp1-1 ura3-1 ade2-1 can1-100*	This study
JBY1395	*MATa mad2-Δ::URA3 rad53-21 his3-11,15 leu2-3,112 trp1-1 ura3-1 ade2-1 can1-100*	This study
JBY1397	*MATa scc1-73 rad53-21 his3-11,15 leu2-3,112 TRP1 ura3-1 ade2-1 can1-100*	This study
JBY1400	*MATa ndc80-1 rad53-21 his3-11,15 leu2-3,112 trp1-1-SPC42-GFP-TRP1 ura3-1 ade2-1 can1-100*	This study

other forms of chromatid association such as topological intertwining (Dewar et al., 2004). These observations suggest that there is actually significant latitude in how KT bi-orientation is achieved. One implication of the work presented here is that budding yeast may have exploited this flexibility to accommodate a cell cycle in which spindle assembly and DNA replication are initiated simultaneously. Such a mode of mitotic control would necessitate a robust mechanism to ensure *CEN* replication when replication fork progression was impeded, providing a selective advantage to a chromosome architecture in which *CEN*s were closely flanked by early firing origins of replication.

Materials and methods

Yeast strains, cell culture, and plasmids

All strains (Table I) are congenic with W303-derived Y300. S. Biggens (Fred Hutchinson Cancer Center, Seattle, WA), K. Bloom (University of North Carolina, Chapel Hill, NC), S. Elledge (Harvard Medical School, Boston, MA), J. Kilmartin (Medical Research Council Laboratory of Molecular Biology, Cambridge, UK), K. Nasmyth (Research Institute of Molecular Pathology, Vienna, Austria), M. Tyers (Samuel Lunenfeld Research Institute, Toronto, Canada), and Y. Wang (Florida State University, Tallahassee, FL) provided strains and reagents that were introduced into the Y300 background using standard yeast genetic techniques. Cells were cultured in yeast extract/peptone/dextrose or synthetic minimal media at 30°C unless otherwise indicated. Cultures for fluorescence microscopy were supplemented with 50 μg/ml adenine. For G_1 synchronization/release experiments, cells were diluted into fresh media, treated with 10 μg/ml α factor, and released at an appropriate temperature ± 200 mM HU (Sigma-Aldrich). p*GAL-CEN6-URA3* was derived from pKF71(Doheny et al., 1993), in which a portion of *ACT1* is fused in frame with LacZ and expressed under control of the *GAL1/10* promoter. The *ACT1* segment contains an intron with a 186-bp *CEN6* CDEI-HI-III insertion flanked by XhoI sites. Oligonucleotides 5′-ATCGGGATCCTTGACGTTAAAGTATAGAGG and 5-ATCGGCGGCCGCCAAGGCGATTAAGTTGGGTAACGCC were used to amplify the *GAL-ACT1-intron:CEN6* region of pKF71, placing a BamHI site upstream of the *GAL* promoter and a NotI site downstream of the *ACT1*::LacZ junction. *URA3* was amplified with oligonucleotides 5′-GATAAAGCGGCCGCAAAGCTACATATAAGG and 5′-GTTTTCCCAGTCACGAC, replacing the *URA3* initiation codon with NotI and incorporating a downstream SacI site. The NotI sites were joined to create a cassette that, after splicing of the *ACT1/CEN6* intron, encodes the first 85 amino acids of Act1, the NH_2-terminal 22 aa of LacZ, and 2–266 aa of Ura3. The *GAL-CEN6-URA3* cassette was transferred into pRS413 (Sikorski and Hieter, 1989) using BamHI and SacI, yielding p*CEN/ARS/HIS3/GAL-CEN6-URA3* (pSK012). XhoI was used to remove *CEN6*, creating p*CEN/ARS/HIS3/GAL-URA3* (pSK013).

Isolation of mutants and two-hybrid screening

To isolate Esh^- strains, Y916 and Y917 were mutagenized to ∼50% survival using ethyl methanesulfonate. 242,700 mutagenized colonies were assayed for sensitivity to 100 mM HU (1,265 strains) and secondarily screened for strains showing a ≥50% reduction in plating efficiency after 8 h of 200 mM HU treatment (123 strains). These strains were examined for an elongated spindle phenotype (spindles ≥3 μm) after 4 h of exposure to 200 mM HU. 43 strains fulfilled this criterion. 26 strains were allelic with *RAD53* and 9 were allelic with *MEC1*. The remaining eight mutants defined four complementation groups. Two-hybrid screening with *SMT4* was performed in PJ69-4a (James et al., 1996) using an *S. cerevisiae* cDNA library constructed by S. Elledge and pJBN84 (p*CEN/ARS/TRP1/ADH-GAL4-DBD-SMT4 R687G, L681A*) as bait. The indicated mutations in pJBN84 were introduced for unrelated reasons and found to permit stable overproduction of the *GAL4-DBD-SMT4* fusion.

Microscopy and cell analysis

Ethanol-fixed cells were stained for flow cytometry with propidium iodide. Cells were processed for α-tubulin immunofluorescence using YOL1/34 (Accurate Scientific) and FITC-conjugated anti–rat secondary antibodies (Sigma-Aldrich). 1 μg/ml DAPI staining was performed in mounting media (Vecta-Shield; Vector Laboratories). *SPC42-GFP* cells were fixed in 4% formaldehyde for 5 min. The distance between *SPC42-GFP* foci was quantified using MetaMorph software. Time-lapse imaging was performed by transferring cells to 2% agarose media pads in a depression chamber slide. Cells were visualized at ambient temperature on an upright microscope (model E800; Nikon) using a 100× Plan Apo 1.4 NA objective. Epifluorescence excitation was performed using a 100-W Hg bulb and a standard FITC bandpass filter cube; a number 8 neutral density filter was used to minimize photobleaching and toxicity. Samples were simultaneously visualized with low levels of bright-field illumination. Stacks of images were acquired at 2-min intervals using a CCD camera (model CoolSNAP fx; Photometrics) and exposure times of ∼200 ms/frame. The focus drive and camera shutters were controlled using the acquisition features of MetaMorph. The distance between *SPC42-GFP* foci was measured within image stacks using the MetaMorph XYZ application. Maximum projections were processed using the "flatten background" algorithm.

Protein techniques

For analysis of Clb2-HA Cdk1, 10 ml of cell cultures at OD_{600} 0.8 were removed for each time point and washed into 1 mM NaN_3, 10 mM EDTA, and 0.9% NaCl. Protein extracts were prepared as described previously (Bachant et al., 2002). 100 μg of the extract was incubated with a 1:100 dilution of 12CA5 α-HA antibody for 12 h at 4°C. Immune complexes were collected using protein A–conjugated Sepharose beads and washed twice in lysis buffer and once in kinase buffer (20 mM Tris 7.5 and 7.5 mM $MgCl_2$). Kinase reactions were assembled by resuspending the immunoprecipitates in 20 μl of kinase buffer, 2 μl of 1 mg/ml histone HI (Sigma-Aldrich), and 1 μl of γ-[^{32}P]ATP (NEN Life Science Products). After incubation at 37°C for 1 h, 4 μl of 6× SDS sample buffer was added and proteins were resolved by SDS-PAGE. Radioactivity incorporated into histone HI was quantified by PhosphoImager (Molecular Dynamics) analysis.

Online supplemental material

Videos 1–5 contain time-lapse sequences of spindle pole dynamics in WT and *rad53-21* mutants exposed to HU. Fig. S1 depicts the kinetics of spindle extension and sister chromatid separation in *mif2* and *mif2mad2* mutants. Online supplemental material is available at http://www.jcb.org/cgi/content/full/jcb.200412076/DC1.

We thank colleagues described in Materials and methods for generously providing strains and other reagents. J. Bachant thanks S. Elledge for support during the formative stages of this work and for encouraging us to try *CENARS* suppression of *rad53*. J. Bachant also thanks S. Elledge and C. Nugent for insightful discussions and anonymous reviewers for suggestions to clarify the manuscript.

This work was supported by a grant from the National Institute of General Medical Sciences (GM-66190) to J. Bachant.

Submitted: 13 December 2004
Accepted: 22 February 2005

References

Agarwal, R., Z. Tang, H. Yu, and O. Cohen-Fix. 2003. Two distinct pathways for inhibiting Pds1 ubiquitination in response to DNA damage. *J. Biol. Chem.* 278:45027–45033.

Alcasabas, A., A. Osborn, J. Bachant, F. Hu, P. Werler, K. Bousset, K. Kanji-Furuya, J.F.X. Diffley, A. Carr, and S.J. Elledge. 2001. Mrc1 transduces DNA replication stress signals to activate Rad53. *Nat. Cell Biol.* 3:958–965.

Allen, J.B., Z. Zhou, W. Siede, E.C. Friedberg, and S.J. Elledge. 1994. The SAD1/RAD53 protein kinase controls multiple checkpoints and DNA damage-induced transcription in yeast. *Genes Dev.* 8:2401–2415.

Bachant, J., A. Alcasabas, Y. Blat, N. Kleckner, and S.J. Elledge. 2002. The SUMO-1 isopeptidase Smt4 is linked to centromeric cohesion through SUMO-1 modification of DNA topoisomerase II. *Mol. Cell.* 9:1169–1182.

Biggins, S., and A.W. Murray. 2001. The budding yeast protein kinase Ipl1/Aurora allows the absence of tension to activate the spindle checkpoint. *Genes Dev.* 15:3118–3129.

Blat, Y., and N. Kleckner. 1999. Cohesins bind to preferential sites along yeast chromosome III, with differential regulation along arms versus the centric region. *Cell.* 98:249–259.

Brinkley, B.R., R. Zinkowski, W. Mollon, F. Davis, M. Pisegna, M. Pershouse, and P.N. Rao. 1988. Movement and segregation of kinetochores experimentally detached from mammalian chromosomes. *Nature.* 336:251–254.

Cheeseman, I.M., M. Enquist-Newman, T. Müller-Reichert, D.G. Drubin, and G. Barnes. 2001. Mitotic spindle integrity and kinetochore function linked by the Duo1p/Dam1p complex. *J. Cell Biol.* 152:197–212.

Cheeseman, I.M., D.G. Drubin, and G. Barnes. 2002. Simple centromere, complex kinetochore: linking spindle microtubules and centromeric DNA in budding yeast. *J. Cell Biol.* 157:199–203.

Ciosk, R., W. Zachariae, C. Michaelis, A. Shevchenko, M. Mann, and K. Nasmyth. 1998. An ESP1/PDS1 complex regulates loss of sister chromatid cohesion at the metaphase to anaphase transition in yeast. *Cell.* 93: 1067–1076.

Clarke, D.J., M. Segal, G. Mondesert, and S.I. Reed. 1999. The Pds1 anaphase inhibitor and Mec1 kinase define distinct checkpoints coupling S phase with mitosis in budding yeast. *Curr. Biol.* 9:365–368.

Clarke, D.J., M. Segal, C. Andrews, S. Rudyak, S. Jensen, K. Smith, and S.I. Reed. 2003. S-phase checkpoint controls mitosis via an APC-independent Cdc20p function. *Nat. Cell Biol.* 5:928–935.

Cohen-Fix, O., J.M. Peters, M.W. Kirschner, and D. Koshland. 1996. Anaphase initiation in *Saccharomyces cerevisiae* is controlled by the APC-dependent degradation of the anaphase inhibitor Pds1p. *Genes Dev.* 10:3081–

3093.

Desany, B., A. Alcasabas, J. Bachant, and S.J. Elledge. 1998. Recovery from DNA replicational stress is the essential function of the S-phase checkpoint. *Genes Dev.* 12:2956–2970.

Dewar, H., K. Tanaka, K. Nasmyth, and T.U. Tanaka. 2004. Tension between two kinetochores suffices for their bi-orientation on the mitotic spindle. *Nature.* 428:93–97.

Doheny, K.F., P.K. Sorger, A.A. Hyman, S. Tugendreich, F. Spencer, and P. Hieter. 1993. Identification of essential components of the *S. cerevisiae* kinetochore. *Cell.* 73:761–774.

Enquist-Newman, M., I.M. Cheeseman, D. Van Goor, D.G. Drubin, P. Meluh, and G. Barnes. 2001. Dad1p, third component of the Duo1p/Dam1p complex involved in kinetochore function and mitotic spindle integrity. *Mol. Biol. Cell.* 12:2601–2613.

Goshima, G., and M. Yanagida. 2000. Establishing biorientation occurs with precocious separation of the sister kinetochores, but not the arms, in the early spindle of budding yeast. *Cell.* 100:619–633.

Guacci, V., D. Koshland, and A. Strunnikov. 1997. A direct link between sister chromatid cohesion and chromosome condensation revealed through the analysis of MCD1 in *S. cerevisiae. Cell.* 91:47–57.

James, P., J. Halladay, and E. Craig. 1996. Genomic libraries and a host strain designed for highly efficient two-hybrid selection in yeast. *Genetics.* 144:1425–1436.

Janke, C., J. Ortiz, T. Tanaka, J. Lechner, and E. Schiebel. 2002. Four new subunits of the Dam1-Duo1 complex reveal novel functions in sister kinetochore biorientation. *EMBO J.* 21:181–193.

Jones, M.H., J. Bachant, A.R. Castillo, T. Giddings, and M. Winey. 1999. Yeast Dam1p is required to maintain spindle integrity and interacts with the Mps1 kinase. *Mol. Biol. Cell.* 10:2377–2391.

Krishnan, V., S. Nirantar, K. Crasta, A. Cheng, and U. Surana. 2004. DNA replication checkpoint prevents precocious chromosome segregation by regulating spindle behavior. *Mol. Cell.* 16:687–700.

Li, S.J., and M. Hochstrasser. 2000. The yeast ULP2 (SMT4) gene encodes a novel protease specific for the ubiquitin-like Smt3 protein. *Mol. Cell. Biol.* 20:2367–2377.

Li, Y., J. Bachant, A.A. Alcasabas, Y. Wang, J. Qin, and S.J. Elledge. 2002. The mitotic spindle is required for loading of the DASH complex onto the kinetochore. *Genes Dev.* 16:183–197.

Lopes, M., C. Cotta-Ramusino, A. Pellicioli, G. Liberi, P. Plevani, M. Muzi-Falconi, C.S. Newlon, and M. Foiani. 2001. The DNA replication checkpoint response stabilizes stalled replication forks. *Nature.* 412:557–561.

McCarroll, R.M., and W.L. Fangman. 1988. Time of replication of yeast centromeres and telomeres. *Cell.* 54:505–513.

Meluh, P.B., and D. Koshland. 1995. Evidence that the MIF2 gene of *Saccharomyces cerevisiae* encodes a centromere protein with homology to the mammalian centromere protein CENP-C. *Mol. Biol. Cell.* 6:793–807.

Michaelis, C., R. Ciosk, and K. Nasmyth. 1997. Cohesins: chromosomal proteins that prevent premature separation of sister chromatids. *Cell.* 91:35–45.

Nekrasov, V.S., M. Smith, S. Peak-Chew, and J.V. Kilmartin. 2003. Interactions between centromere components in *Saccharomyces cerevisiae. Mol. Biol. Cell.* 14:4931–4946.

Piatti, S., C. Lengauer, and K. Nasmyth. 1995. Cdc6 is an unstable protein whose de novo synthesis in G1 is important for the onset of S phase and for preventing a "reductional" anaphase in the budding yeast *Saccharomyces cerevisiae. EMBO J.* 14:3788–3799.

Sanchez, Y., J. Bachant, H. Wang, F. Hu, D. Liu, M. Tetzlaff, and S.J. Elledge. 1999. Control of the DNA damage checkpoint by chk1 and rad53 protein kinases through distinct mechanisms. *Science.* 286:1166–1171.

Santocanale, C., and J.F. Diffley. 1998. A Mec1- and Rad53-dependent checkpoint controls late-firing origins of DNA replication. *Nature.* 395:615–618.

Saunders, W.S., and M.A. Hoyt. 1992. Kinesin-related proteins required for structural integrity of the mitotic spindle. *Cell.* 70:451–458.

Saunders, W., V. Lengyel, and M.A. Hoyt. 1997. Mitotic spindle function in *Saccharomyces cerevisiae* requires a balance of different types of kinesin-related motors. *Mol. Biol. Cell.* 8:1025–1033.

Sikorski, R.S., and P. Hieter. 1989. A system of shuttle vectors and yeast host strains designed for efficient manipulation of DNA in *Saccharomyces cerevisiae. Genetics.* 122:19–27.

Straight, A.F., W. Marshall, J. Sedat, and A.W. Murray. 1997. Mitosis in living budding yeast: anaphase A but no metaphase plate. *Science.* 277:574–578.

Tanaka, T.U., N. Rachidi, C. Janke, G. Pereira, M. Galova, E. Schiebel, M. Stark, and K. Nasmyth. 2002. Evidence that the Ipl1-Sli15 (Aurora kinase-INCENP) complex promotes chromosome bi-orientation by altering kinetochore-spindle pole connections. *Cell.* 108:317–329.

Thrower, D.A., and K. Bloom. 2001. Dicentric chromosome stretching during anaphase reveals roles of Sir2/Ku in chromatin compaction in budding yeast. *Mol. Biol. Cell.* 12:2800–2812.

Wang, H., D. Liu, Y. Wang, J. Qin, and S.J. Elledge. 2001. Pds1 phosphorylation in response to DNA damage is essential for its DNA damage checkpoint function. *Genes Dev.* 15:1361–1372.

Weinert, T.A., G.L. Kiser, and L.H. Hartwell. 1994. Mitotic checkpoint genes in budding yeast and the dependence of mitosis on DNA replication and repair. *Genes Dev.* 8:652–665.

Yabuki, N., H. Terashima, and K. Kitada. 2002. Mapping of early firing origins of a replication profile of budding yeast. *Genes Cells.* 7:781–789.

Yamamoto, A., V. Guacci, and D. Koshland. 1996. Pds1p, an inhibitor of anaphase in budding yeast, plays a critical role in the APC and checkpoint pathway(s). *J. Cell Biol.* 133:99–110.